PRELIMINARY TESTS FOR SPECKLE-BASED X-RAY PHASE-CONTRAST IMAGING: OPTIMIZATION

Laura-Anamaria Nita[1], Mihai Iovea[2], Gabriel Suliman[3], Alexandru Enciu[4] and Marian Neagu[5]

This paper presents the optimization of a speckle-based X-ray phase-contrast imaging setup. There are reported advances in techniques from the creation of a random speckle pattern to its characterization; the process of choosing the most suitable diffuser based on the patterns obtained using different types of phase-modulators; our experimental setup along with a discussion about its limitations and how to overcome them and we describe the procedure we implemented for speckle characterization and information retrieval from the acquired images. The obtained results are promising being comparable with thoses previously reported in literature.

Keywords: X-ray phase-contrast imaging, X-ray speckle-based imaging

1. Introduction

X-ray phase-contrast imaging (XPCI) is a non-destructive technique that was developed to overcome the limitations inherent to the traditional methods based on X-ray absorption[1]. In absorption-based X-ray imaging, especially in samples with limited composition variation like biological samples, the features that present similar densities are indistinguishable. The phase-contrast imaging method is based on the fact that these features will generally induce a much more varied shift on the phase of the X-ray wave as it travels through the sample. By investigating the variations in the phase of the outgoing X-ray we can obtain phase-contrast images, whose interpretation gives us complementary information to the absorption images of the sample [2], [3]. XPCI techniques have demonstrated their value through the years having been used in a wide range of domains from biomedical investigations to pre-clinical and clinical imaging [4] - [14], material science [15] - [18] and metrology.

The phase-contrast methods were first implemented for electromangentic waves in the visible domain [19] and they were extended to the X-ray domain about 30 years later [20]. This development was made possible by the construction of large synchrotron facilities that provided brilliant, coherent and monochromatic X-ray beams[20]. To farther improve the availability of these methods, many efforts have been made to use them with polychromatic and divergent stand-alone laboratory sources. [21], [22], [23].

The implementation of phase-contrast X-ray imaging is quite troublesome since it implies the use of a parameter that is not directly measurable by any type of detector: the

[1]Physics Department, University Politehnica of Bucharest, Splaiul Independentei No. 313, 060042 Bucharest-Sector 6, Romania, e-mail: laura_anamaria.nita@upb.ro

[2]Accent Pro 2000 SRL, Nerva Traian Nr. 01 K6, Ap. 26, Sector 3, 031041 Bucharest, Romania, e-mail: office@accent.ro

[3]Physics Department, University Politehnica of Bucharest, Splaiul Independentei No. 313, 060042 Bucharest-Sector 6, Romania, e-mail: gabriel.suliman@upb.ro

[4]Accent Pro 2000 SRL, Nerva Traian Nr. 01 K6, Ap. 26, Sector 3, 031041 Bucharest, Romania, e-mail: office@accent.ro

[5]Accent Pro 2000 SRL, Nerva Traian Nr. 01 K6, Ap. 26, Sector 3, 031041 Bucharest, Romania, e-mail: office@accent.ro

phase of the electromagnetic radiation. Several phase-sensitive imaging techniques have been developed [4]: grating-interferometry [11], which requires expensive optical elements and has low experimental setup flexibility [1]; propagation based imaging [2], which needs high-resolution detectors and presents lower sensitivity to the phase-shift induced by the sample [1]; X-ray speckle-based imaging, which has a simple and flexible experimental geometry, is cost-effective compared to the other methods, and has relatively low spatial and temporal coherence requirements [1], [24].

In this paper we are presenting the first results in implementing the X-ray speckle-based imaging method at the laboratory of Accent PRO 2000 SRL. Section 2 decribes the principle of the method, section 3 presents the details of our experimental implementation and its optimization, while chapter 4 presents our data analysis procedure and our results.

2. Speckle-based phase-contrast imaging

In speckle-based X-ray imaging the plane electromagnetic wavefront is being transformed when it passes through a diffuser. When viewed on an imaging detector the diffuser induces the appearance of local intensity maxima named speckles, which replace an ideal uniform intensity distribution. When an object is added in the path of the X-rays, these speckles are changing position according to the refraction index of the object. In order to extract the information about the object, the two images, one with object and one without the object are being compared and the displacement of the speckles measured.

2.1. **Speckle pattern characterization.** The first aspect that needs to be addressed in speckle-based X-ray imaging is the process of obtaining the speckle pattern. To create a speckle pattern one needs a partially coherent X-ray beam illuminating an object consisting of randomly distributed and negligibly absorbing features, called a diffuser. The diffuser can be a piece of sandpaper, finely ground sand, glass or even biological filter membranes with micrometer-sized pores [1]. As the beam impinges on the diffuser the X-ray wavefront is distorted, as shown in figure 1. When viewed using an imaging detector, the randomly distributed scatterers create both convergent and divergent zones which will result in the creation of a random pattern of low and high intensity pixels that is named speckle pattern.

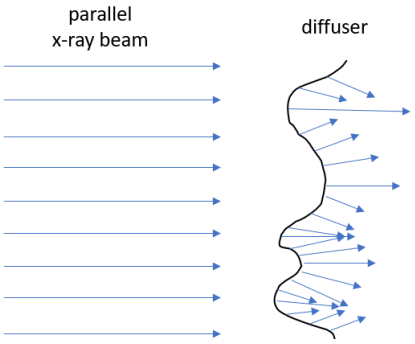

FIGURE 1. Representation of a parallel X-ray beam incident on a diffuser thus modulating the wavefront of the beam and creating a random speckle pattern.

Speckle-based imaging techniques are mostly used in the near-field regime, although the speckles can also appear in the far-field one [25]. In this paper we will discuss only the near-field regime. The near-field speckle-pattern can be described using the size of the

speckles, which is dictated by the size of the distortions presented in the diffuser, and using the visibility of the speckle pattern which is determined only by the shape of the wavefront, both having a significant influence on the quality of the reconstructed images [26].

The speckle size is determined by the size of the scattering particles in the diffuser, and, since these are of various sizes and are randomly distributed, we can only estimate an average size of the speckles. This can be done with the help of a two-dimensional autocorrelation of the speckle pattern, from which we consider the full width at half maximum (FWHM) of the autocorrelation peak as a measure for the speckle size.

The visibility or contrast of the speckle pattern ([23], [27] - [29]) is defined as the ratio between the standard deviation, σ_I, and the mean intensity value of the speckle pattern, $\overline{I}$, calculated in a small region of interest (in general with dimensions around 150 x 150 pixels):

$$v = \frac{\sigma_I}{\overline{I}} \tag{2.1}$$

While other definitions of the visibility are possible [21], [22], [28], this definition is more suitable for our measurements because the outliers have a low impact on the result. Other definitions, which make use of the maximum and minimum intensity values of the speckle pattern, are sensitive to the fluctuations in pixel illumination between different acquisitions yielding unreliable visibility values when the statistics is low.

2.2. **Experimental setup.** The experimental setup of speckle-based X-ray imaging is surprisingly simple, intuitive and inexpensive. The arrangement consists of an X-ray source, a diffuser, a sample to be analyzed and a detector. This setup can easily be applied to both parallel and divergent beams [21], [23]. A schematic implementation of the arrangement is shown in figure 2.

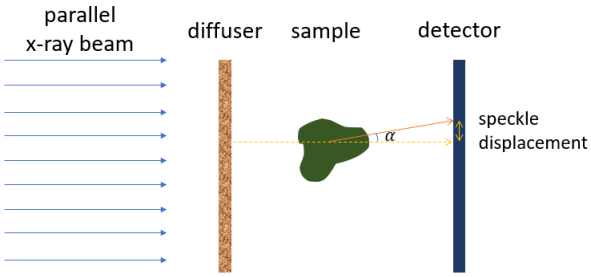

FIGURE 2. Schematic representation of an X-ray speckle-based imaging experiment.

The X-ray beam impinges on the diffuser (phase modulator) creating a random speckle pattern, in the way that has already been discussed in the previous sub-chapter. This image is called the reference interference pattern. When a sample is placed downstream of the diffuser it modulates the initially recorded speckle pattern in position, intensity and visibility. The position modulation manifests as a displacement of the speckles both in the horizontal and vertical directions, caused by the refraction suffered by the X-rays that travel through the sample. Consequently the speckles obtained from the rays that do not interfere with the sample will have the same position as in the reference pattern. The intensity and visibility modulations are due to the increased absorption caused by the sample, which in turn will render as change in the mean intensity.

The displacement of speckles is described by a vector $\mathbf{u} = (u_x, u_y)$, where u_x and u_y represent the displacement values in horizontal and vertical directions, respectively. The

displacement $\mathbf{u}$ is directly linked to the refraction angle $\boldsymbol{\alpha} = (\alpha_x, \alpha_y)$ through simple geometry. This angle can be converted into the differential phase-shift $(\partial\phi/\partial x, \partial\phi/\partial x)$, where ϕ reprezents the phase [30]:

$$\frac{\partial\phi}{\partial x} = \frac{2\pi}{\lambda}\alpha_x, \qquad \frac{\partial\phi}{\partial y} = \frac{2\pi}{\lambda}\alpha_y \tag{2.2}$$

where λ is the X-ray wavelength. The phase-shift of the wavefront is then obtained by integrating the differential phase signals in the two orthogonal directions, which can be done in different ways: Fourier-based methods [31] - [34], two-dimensional numerical integration using least-squares minimization [35], [36], or matrix inversion [28].

Two more images can be retrieved from the images acquired with this experimental arrangement:

- the transmission image $\mathbf{T}$, given as the ratio between the measured local intensities in the sample and reference interference pattern, is the equivalent of the traditional absorption image. The difference is that it also contains edge-enhancement effects specific for the near-field regime.
- the dark-field signal $\mathbf{D}$, obtained as the ratio between the visibilities of the sample and reference interference patterns, measures the local reduction in amplitude of the speckle pattern.

3. Experimental implementation and data acquisition

3.1. Implementation of the experimental setup. The experiment was conducted using a XWT-100-THE microfocus X-ray generator [37] having a maximum voltage of 160 kV, 1 mA and a $3\mu m$ focal spot. For the phase modulator we tested out different types of commercial sandpaper with various granulations, lead powder and even granulated sugar. The detection system was composed of a Hamamatsu C9100-23B camera [38], a CsI scintillator and a mirror placed at 45 degrees between the previous two elements, as a means of recording the image without exposing the camera sensor to direct radiation. A 3 mm thickness lead screen protector was mounted around the camera to protect its sensitive elements. An additional 30 mm diameter lead cylinder having a 35 mm height shields the lens of the camera. An image of the detection system is presented in figure 3.

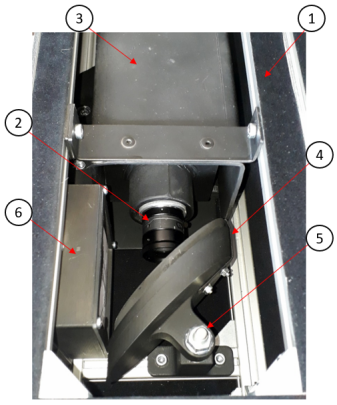

FIGURE 3. Image of the detection system composed of: (1) Aluminium case; (2) Camera lens; (3) Lead protection screen; (4) Mirror; (5) Angular adjustment mechanism; (6) CsI scintillator screen.

The geometric arrangement of the setup is sketched in figure 4 (a) and a photo of it is shown in 4 (b). The diffuser was placed at 56 cm from the x-ray source and 25 cm from the detector plane, resulting in a 1.45 magnification of the diffuser features at the detector plane. The sample was introduced in the arrangement at 11 cm downstream of the phase modulator, leading to a magnification of approximately 1.16.

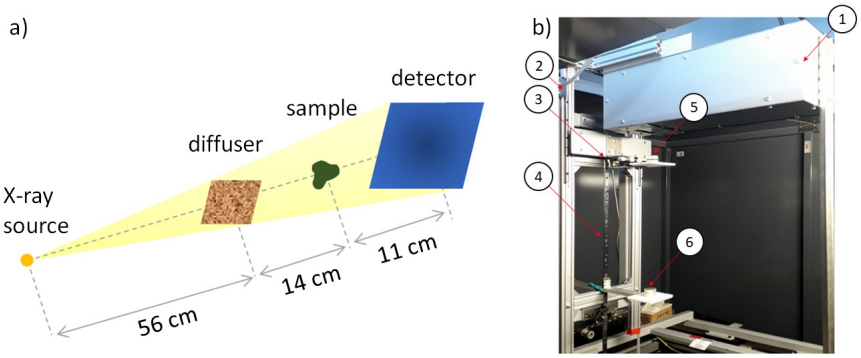

FIGURE 4. (a) Sketch of the geometric arrangement of the experimental setup. (b) Laboratory photo of the experimental setup: (1) detection system (Hamamatsu camera, CsI scintillator and 45 degree mirror); (2) guide rails for supporting and moving the detector; (3) driver for stepper motor operation; (4) vertical translation axis for positioning the sample and the diffuser; (5) sample mount; (6) diffuser mount.

To have a reference point in the sample image and to help determine the resolution of the camera we place two copper wires intersecting close to the sample, each of them having a 0.2 mm diameter. These two wires can easily be seen as they provide enough absorption (figure 5). Knowing the diameter of the copper wire and measuring thickness of the "shadow" it left at the detector plane, we calculated the pixel size as the ratio between these two values obtaining the best possible achievable resolution of roughly 2.5 μm.

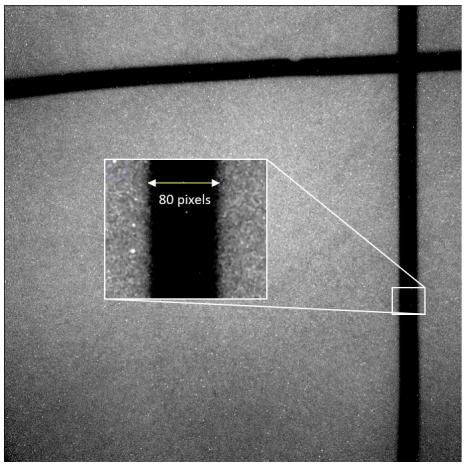

FIGURE 5. Image of the speckle pattern with the cross-copper wires used for determining the camera resolution.

We measured the resolution of the scintillator by determining the LPM (line pairs per mm) with the use of an indicator with values between 5 and 20. The obtained value was 20 LPM, which is also the maximum possible value for our indicator. This results in a 25 μm resolution of the scintillator, which is ten times larger than what we could have achieved with the camera. This resolution limitation induced by the scintillator, affects the quality of the acquired images.

3.2. **Data acquisition.** The parameters at which the X-ray generator was operated were: 45 keV acceleration voltage and 100 μA beam current. Each image was obtained from averaging 20 frames, each of them aquired with an exposure time of 5s.

We analyzed the quality of the speckle patterns obtained with all the phase modulators mentioned above. Samples from the collected images are shown in figure 6, along with a close-up of the pattern obtained with the lead powder, where the speckles are best visible. The lead powder, which has a 40 to 70 microns grain size, was used as a phase-modulator for the rest of the measurements. To induce a phase contrast, a small piece of leaf was used as sample.

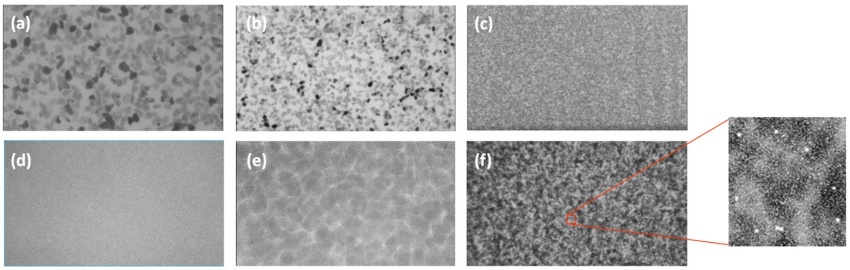

FIGURE 6. Speckle patterns acquired with different types of phase modulators: (a) P40 sandpaper; (b) P80 sandpaper; (c) P280 sandpaper; (d) P600 sandpaper; (e) granulated sugar; (f) 40-70 microns sized lead powder along with a zoomed in small Region of Interest.

4. Data analysis

Both the reference and sample images are usually corrected for the offset (the image acquired without turning on the X-ray source, representing the noise). Because of the low signal provided by the scintillator, we were unable to make this correction, as the values measured for the offset image are very close to the values obtained when the source is turned on. This results in statistical fluctuations which would introduce great errors if the correction was made. To overcome this impediment, longer exposure times are needed for every acquisition. Due to this fact, the analysis was performed on uncorrected images.

4.1. **Speckle characterization.** Speckle visibility and size are a measure of the capabilities of the experimental setup. The speckle visibility was determined via equation **2**.1 by averaging the results obtained for multiple regions-of-interest (ROI) in the reference image. The average speckle visibility has a value of $v = (13.8 \pm 1.6)\%$, which is comparable with the visibilities obtained with similar setups presented in literature [24], [39].

The average speckle size was extracted from the two-dimensional autocorrelation of the reference pattern by considering the full width at half maximum (FWHM) of the autocorrelation peak [39]. This was obtained by profiling a line though the center of the 2D autocorrelation image for both horizontal and vertical axes. The measured speckle size was

approximately 1.3 pixels in both horizontal and vertical direction. These values are a little lower than the general speckle size encountered in literature [24].

4.2. Displaced speckle identification. To identify the speckles that have been displaced because of the different refraction index induce by the presence of the sample in the trajectory of the X rays, we developed an algorithm which was ran as a macro in Image J [40], a java-based image processing program. The algorithm has the following steps:

1. Set the threshold for the pixel values that are supposed to be speckles, which was chosen by analyzing the histogram of the reference image, and a specific minimum size for the speckles.
2. Search the reference image for "clusters" that have pixel values above the previously set threshold and meet the specified minimum size.
3. Once a speckle is identified, make a window of 80 x 80 pixels around it.
4. Extract the same window (same size and position) from the sample image.
5. In the sample image, search for the previously identified speckle.
6. If found, calculate the displacement of the speckle between the reference window and the sample window, in both directions.
7. Through simple geometry, determine the refraction angles for horizontal and vertical directions, which are directly linked to the phase shift (equation **2**.2).

Figures 7 and 8 present examples of such identified displaced speckles. In figure 7 the displacement took place in both horizontal and vertical directions having values of 5 and 3 pixels, respectively. From this, knowing the distance between the sample and the detector, we were able to calculate the refraction angles as:

$$\alpha_x = \frac{u_x}{d}, \alpha_x = \frac{u_y}{d} \tag{4.1}$$

where d is the distance from the sample to the detector. For this example the calculated refraction angles had values of 1.98 μrad for the horizontal displacement and 1.18 μrad for the vertical displacement.

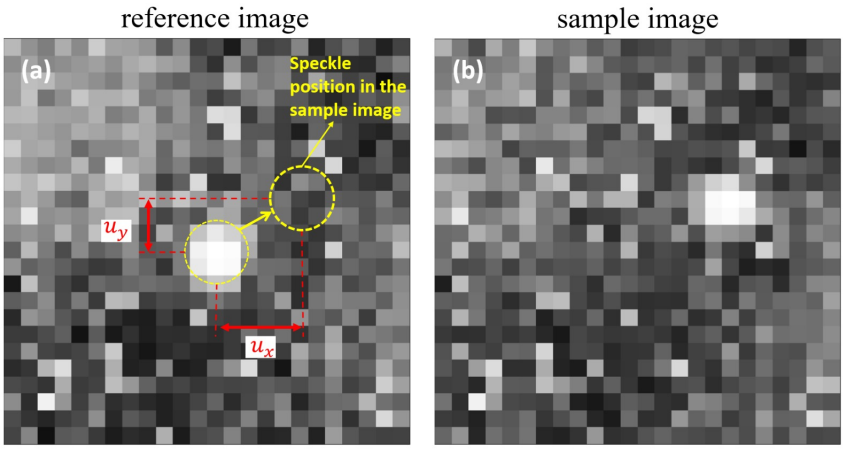

FIGURE 7. Displaced speckle illustrated in the reference image (a) and in the sample image (b). The displacement in the horizontal and vertical directions are represented as u_x and u_y, respectively.

From all the speckles that were found in the reference image, approximately 12% of them were associated with a speckle at a different position in the sample image and thus

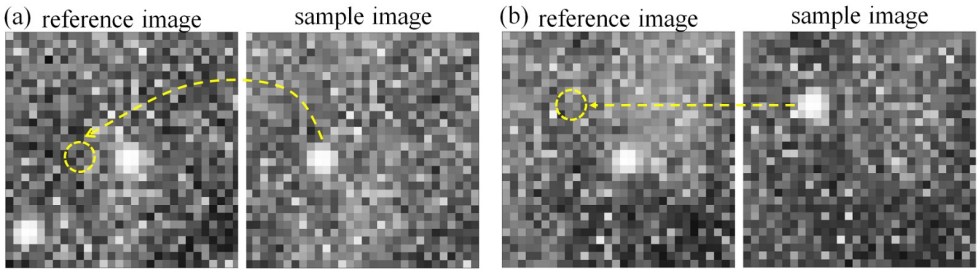

FIGURE 8. Examples of displaced speckles. (a) horizontal displacement; (b) horizontal and vertical displacement.

identified as a displaced speckle. This is in accordance with our experimental implementation giving that the sample represents a small percentage of the field of view. The average values of the displacements and the refraction angles, calculated in both directions, are presented in table 1. The results obtained with this experimental setup are comparable with those achieved in another experiment conducted with a similar setup [24].

TABLE 1. Average values of the displacement and the refraction angle as obtained in the present work.

Horizontal displacement [pixels]	Vertical displacement [pixels]	Horizontal refraction angle [μrad]	Vertical refraction angle [μrad]
8.85	7.75	3.40	3.07

5. Conclusions

This paper presents an implementation of a phase-contrast method in the X-ray regime. It describes the experimental setup, a discussion of the diffuser and the algorithm that is used for analysing the experimental data. We characterize the speckles and, using a simple object, we show that the algorithm is able to identify displaced speckles. From the displacement values, both the horizontal and vertical refraction angles are measured. The obtained values are comparable to the values previously reported in literature.

The experiment shows that the phase-contrast method can be used in our experimental setup and show promising results despite some identified weak points like the intensity of the source, that has great impact on the statistics of the experiment and the choice of scintilator that limits the resolution of the images. We show the first optimisation steps in the choice of the diffuser type and material and we conclude that the best choice in our experimental conditions is a diffuser made of lead microstructures. The experimental set-up is implemented in the laboratory of Accent PRO 2000 SRL.

Acknowledgements

The X-ray set-up development have been financed from the subsidiary Contract nr. 139/27.09.2016-Competitivity Operational Program 2014-2020, co-funded from the European Fund for Regional Development and the Ministry of Investment and European Projects.

REFERENCES

[1] *M.-C. Zdora*, State of the Art of X-ray Speckle-Based Phase-Contrast and Dark-Field Imaging, J. Imaging **4**, 60 (2018).

[2] *S.W. Wilkins, T. E. Gureyev, D. Gao, A. Pogany, A.W. Stevenson*, Phase-contrast imaging using polychromatic hard x-rays, Nature **384** (2009), 335-337.

[3] *A. Snigirev, I. Snigireva, V. Kohn, S. Kuznetsov, I. Schelokov*, On the possibilities of x-ray phase contrast microimaging by coherent high-energy synchrotron radiation, Rev. Sci. Instrum. **66** (1995), 5486-5492.

[4] *A. Momose*, Recent Advances in X-ray Phase Imaging, Jpn. J. of Appl. Phys. **44** (2005), 6355.

[5] *R. Fitzgerald*, Phase-Sensitive X-ray Imaging, Phys. Today **43** (2000), 23.

[6] *R.A. Lewis*, Medical phase contrast X-ray imaging: Current status and future prospects, Phys. Med. Biol. **49** (2004), 3573.

[7] *O. Betz, U. Wegst, D. Weide, M. Heethoff, L. Helfen, W.-K. Lee, P. Cloetens*, Imaging applications of synchrotron X-ray phase-contrast microtomography in biological morphology and biomaterials science. I. General aspects of the technique and its advantages in the analysis of millimetre-sized arthropod structure, J. Microsc. **227** (2007), 51-71.

[8] *I. Williams, K. Siu, G. Runxuan, X. He, S. Hart, C. Styles, R. Lewis*, Towards the clinical application of X-ray phase contrast imaging, Eur. J. of Radiol. **68** (2008), S73-S77.

[9] *S.-A. Zhou, A. Brahme*, Development of phase-contrast X-ray imaging techniques and potential medical applications, Phys. Med. **24** (2008), 129-148.

[10] *A. Bravin, P. Coan, P. Suortti*, X-ray phase-contrast imaging: From pre-clinical applications towards clinics, Phys. Med. Biol. **58** (2013), R1.

[11] *P. Coan, A. Bravin, G. Tromba*, Phase-contrast X-ray imaging of the breast: Recent developments towards clinics, J. Phys. D **46** (2013), 494007.

[12] *T. Koehler, H. Daerr, G. Martens, N. Kuhn, S. Löscher, U. van Stevendaal,E. Roessl*, Slit-scanning differential X-ray phase-contrast mammography: Proof-of-concept experimental studies, Med. Phys. **42** (2015), 1959-1965.

[13] *F. Horn, C. Hauke, S. Lachner, V. Ludwig, G. Pelzer, J. Rieger, M. Schuster, M. Seifert, J. Wandner, A. Wolf, et al.*, High-energy X-ray grating-based phase-contrast radiography of human anatomy, Proc. SPIE (2016), 9783.

[14] *A. Momose, W. Yashiro, K. Kido, J. Kiyohara, C. Makifuchi, T. Ito, S. Nagatsuka, C. Honda, D. Noda, T. Hattori, et al.e*, X-ray phase imaging: From synchrotron to hospital, Philos. Trans. Royal Soc. A **372** (2014), 20130023.

[15] *P. Cloetens, M. Pateyron-Salomé, J.Y. Buffière, G. Peix, J. Baruchel, F. Peyrin, M. Schlenker*,Observation of microstructure and damage in materials by phase sensitive radiography and tomography, J. Appl. Phys. **81** (1997), 5878-5886.

[16] *A.W. Stevenson, T.E. Gureyev, D. Paganin, S.W. Wilkins, T. Weitkamp, A. Snigirev, C. Rau, I. Snigireva, H.S. Youn, I.P. Dolbnya, et al.*, Phase-contrast X-ray imaging with synchrotron radiation for materials science applications, Nucl. Instr. Meth. Phys. Res. B **199** (2003), 427-435.

[17] *B. Zoofan, J.-Y. Kim, S.I. Rokhlin, G.S. Frankel*, Phase-contrast X-ray imaging for nondestructive evaluation of materials, J. Appl. Phys. **100** (2006), 014502.

[18] *S.C. Mayo, A.W. Stevenson, S.W. Wilkins*, In-Line Phase-Contrast X-ray Imaging and Tomography for Materials Science, Materials **5** (2012), 937-365.

[19] *F. Zernike*, Phase contrast, a new method for the microscopic observation of transparent objects, Physica **9** (1942), 686-698.

[20] *U. Bonse, M. Hart*, An X-ray interferometer, Appl. Phys. Lett. **6** (1965), 155-156.

[21] *I. Zanette, T. Zhou, A. Burvall, U. Lundström, D. H. Larsson, M. Zdora, P. Thibault, F. Pfeiffer, and H. M. Hertz*, Speckle-Based X-Ray Phase-Contrast and Dark-Field Imaging with a Laboratory Source, Phys. Rev. Lett. **112**, 253903 (2014).

[22] *S.Tunhe Zhou, I. Zanette, M.-C. Zdora, Ulf Lundström, Daniel H. Larsson, Hans M. Hertz, Franz Pfeiffer, Anna Burvall*,Speckle-based X-ray phase-contrast imaging with a laboratory source and the scanning technique, Opt. Lett. **40** (2015), 2822–2825.

[23] *H. Wang, Y. Kashyap, K. Sawhney*, From synchrotron radiation to lab source: Advanced speckle-based X-ray imaging using abrasive paper, Sci. Rep. **6** (2016), 20476.

[24] *M.-C. Zdora, I. Zanette, T. Walker, N. W. Phillips, R. Smith, H. Deyhle, S. Ahmed, P. Thibault*, X-ray phase imaging with the unified modulated pattern analysis of near-field speckles at a laboratory source, Appl. Opt. Vol. 59, No. 8 (2020).

[25] *V. Parigi, E. Perros, G. Binard, C. Bourdillon, A. Maître, R. Carminati, V. Krachmalnicoff, Y. De Wilde*, Near-field to far-field characterization of speckle patterns generated by disordered nanomaterials, Opt. Express **7** (2016), 7019-7027.

[26] *R. Cerbino, L. Peverini, M.A.C. Potenza, A. Robert, P. Bösecke, M. Giglio*, X-ray-scattering information obtained from near-field speckle, Nat. Phys. **4** (2008), 238-243.

[27] *D. Magatti, A. Gatti, F. Ferri*, Three-dimensional coherence of light speckles: Experiment, Phys. Rev. A **79** (2009), 053831.

[28] *S. Berujon, E. Ziegler*, X-ray Multimodal Tomography Using Speckle-Vector Tracking, Phys. Rev. Appl. **5** (2016), 044014.

[29] *H. Wang, Y. Kashyap, B. Cai, K. Sawhney*, High energy X-ray phase and dark-field imaging using a random absorption mask, Sci. Rep. **6** (2016), 30581.

[30] *D.M. Paganin, D. Pelliccia*, X-ray phase-contrast imaging: a broad overview of some fundamentals, Advances in Imaging and Electron Physics **218** (2021), 63-158.

[31] *K.S. Morgan, D.M. Paganin, K.K.W Siu*, X-ray phase imaging with a paper analyzer, Appl. Phys. Lett. **100** (2012), 124102.

[32] *S. Berujon, H. Wang, I. Pape, K. Sawhney*, X-ray phase microscopy using the speckle tracking technique, Appl. Phys. Lett. **102** (2013), 154105.

[33] *C. Kottler, C. David, F. Pfeiffer, O. Bunk*, A two-directional approach for grating based differential phase contrast imaging using hard X-rays, Opt. Express **15** (2007), 1175-1181.

[34] *R.T. Frankot, R. Chellappa*, A method for enforcing integrability in shape from shading algorithms, IEEE Trans. Pattern Anal. Mach. Intell. **10** (1988), 439-451.

[35] *S. Berujon, E. Ziegler, P. Cloetens*, X-ray pulse wavefront metrology using speckle tracking, J. Synchrotron Radiat. **22** (2015), 886-894.

[36] *M. Harker, P. O'Leary*, Least squares surface reconstruction from measured gradient fields, IEEE Conference on Computer Vision and Pattern Recognition, Anchorage, AK, USA, (2008), 1063-6919

[37] www.x-ray-worx.com/

[38] www.hamamatsu.com/eu/en/product/cameras/emccd-cameras/C9100-23B.html/

[39] *I. Zanette, M.-C. Zdora, T. Zhou, A. Burvall, D. H. Larsson, P. Thibault, H. M. Hertz, F. Pfeiffer*, X-ray microtomography using correlation of near-field speckles for material characterization, Proc. Natl. Acad. Sci. USA **122** (2015), 12569-12573.

[40] *C.A. Schneider, W.S. Rasband, K.W. Eliceiri*, NIH Image to ImageJ: 25 years of image analysis, Nat. Meth. **9** (2012), 671-675.